Lidar Observations of the Convective Boundary Layer

K. E. KUNKEL, E. W. ELORANTA AND S. T. SHIPLEY

Department of Meteorology, University of Wisconsin, Madison 53706

(Manuscript received 16 May 1977, in revised form 20 September 1977)

ABSTRACT

A scanning lidar system has been used to observe convection in the atmospheric boundary layer. In particular, cell sizes and geometry have been determined and circulation patterns in and around the cells have been measured.

The lidar data show that the preferred form of convective cells are plumes with roots near the surface. The majority of these plumes have aspects ratios between 0.5 and 1.5. The measurements of circulation patterns show the strongest rising motion on the upwind side of the cell with sinking motion on the downwind side. These observations show that lidar is a powerful tool for observing convection.

1. Introduction

Clear air convective plumes are both too large and too short-lived to be easily observed with conventional meteorological instrumentation. Typical cells have altitudes on the order of 1 km and lifetimes of much less than 1 h. The most successful studies have used instrumented aircraft to observe a field of cells (Lenschow, 1970; Warner and Telford, 1963, 1964, 1967) and/or very high power radars to map plumes by observing the changes in radio refractive index which occur at cell boundaries (Konrad, 1970; Konrad and Robinson, 1972, 1973; Hardy and Ottersten, 1969; Rowland, 1973, 1976).

This paper shows how lidar, the optical equivalent of radar, can be used to make detailed observations of developing convective cells. In the atmospheric boundary layer, the principal scattering sources for the lidar signal are aerosols and air molecules. Aerosol particulates are introduced into the atmosphere from a variety of sources, including windblown dust and man-made pollution sources. Most of these sources are at or near the earth's surface. Particulate matter which is injected into the air during the night is usually trapped in a thin layer near the ground. After sunrise, solar heating produces convective cells which transport these aerosols aloft. Lidar is able to give a two-dimensional picture of relative aerosol concentration, and the convective cells can therefore be identified by their higher aerosol concentration.

Lidar possesses several advantages in observing the convective field over other methods. Unlike airplane and tower measurements, lidar is able to give essentially instantaneous two-dimensional pictures of convection. This capability is also possessed by radar. According to Konrad (1970), however, radar apparently can observe cells only at the top of the convective field where they have negative buoyancy and are cool and moist compared to the environment. In light wind situations, lidar is frequently able to observe cells nearly to the surface. Mechanical turbulence appears to mix surface layer dust under windy conditions, and convective structures can no longer be observed near the ground with the current instrumentation. Under these conditions, however, cells can still be observed some distance above the surface. The data presented here were collected from the Meteorology and Space Science Building at the University of Wisconsin with the lidar pointing west over a primarily residential area of Madison. It should therefore be kept in mind that the results may include effects due to the inhomogeneous nature of the urban terrain.

2. Instrumentation and method

The observations presented in this paper were made with a computer controlled scanning ruby lidar system. The system has a maximum repetition rate of 1 Hz at a pulse energy of 1.5 J and a range resolution of 15 m.

In a typical observation period the lidar system is scanned under computer control through a sequence of elevation angles (RHI scan) or of azimuth angles (PPI scan) (see Kunkel *et al.*, 1975). Individual lidar profiles are logarithmically amplified, digitized at a 10 MHz rate, and transferred to an on-line computer for processing. Each lidar profile consists of 512 digital values of the range and energy corrected signal specified at 15 m range intervals. Each value is proportional to the logarithm of the product $\beta'_{180}(r)\exp[-2\tau(r)]$, where $\beta'_{180}(r)$ is the volume backscatter cross section at range r and $\tau(r)$ is the optical thickness between the laser and the scattering volume. Aerosol carried within convec-

tive plumes increases the value of β'_{180} with respect to a background level and thus the plume becomes visible to lidar probing. To produce the pictures shown in this paper, the digital values from a sequence of lidar profiles comprising one angular scan are used to specify intensities at each point in a 500×672 picture array. Since the sequence of lidar profiles consist of an angular scan with individual profiles separated by typical angles of 0.5°, not all elements of the picture array have corresponding values in the profiles. The intermediate points in the picture array are therefore generated by a linear interpolation between the nearest lidar data points. A background level which was taken to be the signal level above the inversion is subtracted from all data points to enhance the contrast. When appreciable attenuation is present, a background level which decreases linearly with range is used to approximately correct for attenuation. On the clear blue sky days considered in this study, however, the optical thickness τ was small and attenuation effects could usually be neglected.

The enhanced picture arrays were then stored on a 9-track digital magnetic tape in a format suitable for display on the McIDAS (Smith, 1975) image display and processing system. McIDAS allows video display of the lidar picture array while providing flexible operator control over grey scale enhancements, picture magnification and false color enhancements as well as sequential display of frames to produce motion pictures. Fig. 1 is an example of an RHI picture as shown on the McIDAS video display. These data were collected on 28 September 1976 and show a variety of convective structures. The contrast here between the convective structures and the surrounding environment is large. Fig. 2 shows an RHI scan taken on 22 October 1976. In this case convection is occurring under a strong capping inversion at a height of 0.8 km. Here the contrast is much smaller. The dip in the inversion at a range of 3.7 km is caused by the plume at a range of 4.0 km.

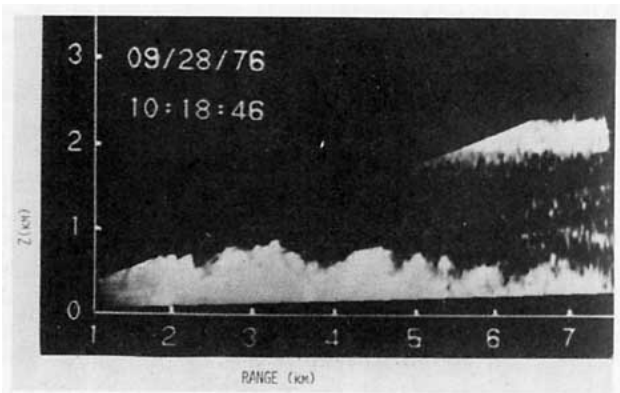

FIG. 1. RHI scan taken at Madison, Wisc., on 28 September 1976 at 1010 CDT.

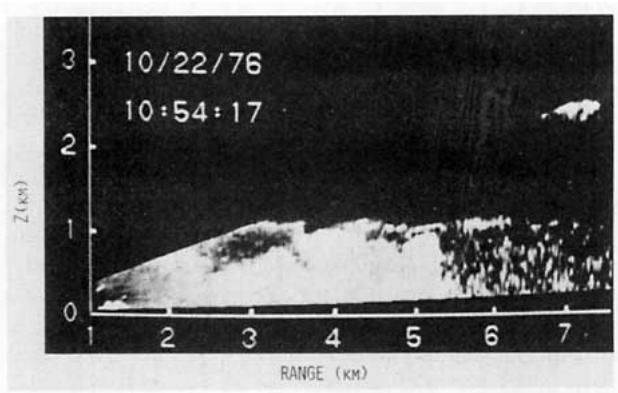

FIG. 2. RHI scan taken on 22 October 1976 which shows dips in the inversion at a range of 3.7 km due to plume at 4.0 km. Mean wind is to the left at 6.5 m s^{-1}.

3. General features of convective field

Controversy exists as to whether the individual convective elements are plume structures or bubbles. Airplane measurements by Warner and Telford (1963, 1967) and acoustic sounder observations by Hall (1972), among others, support a plume model. In contrast, radar observations by Hardy and Ottersten (1969), Konrad (1970) and Rowland (1976) show dome-like structures which Rowland interprets as bubbles.

In the lower part of the boundary layer, lidar RHI scans indicate that the most frequently occurring convective structure is a plume which has roots at or near the surface. These plumes on occasion have been observed to reach heights of 1500 m and still maintain their plume structure. The vertical velocity of the top of the plume is generally of the order of 1 m s^{-1} or more. We conclude from these observations that the plume structures are the primary mechanism for the vertical transport of heat near the surface. We also observe dome-like structures near the inversion top in the mature convective boundary layer. These structures probably correspond to the radar observed "bubbles." However, we hesitate to identify these structures with bubble convection models such as that of Scorer and Ludlam (1953).

The size of these convective elements as measured in other investigations is quite variable ranging from 100 m observed by Vulf'son (1961) to as large as 2 km according to Konrad (1970). The lidar observations were used to measure the horizontal dimensions of the convective elements. Only convective elements with distinct boundaries and a coherent structure extending at least 150 m in the vertical were considered. The vertical dimension of these structures was always measured from the surface, and the diameter was measured at the point of largest horizontal extent. In some cases these plumes could be identified as distinct entities nearly to the surface. In other cases where the boundary layer was

well mixed, the plumes could only be seen where they intruded into the clear air above the inversion.

There are certain biases which may be present in the resulting measurements. Since the lidar sees a vertical slice through the plume, it will in general underestimate the size. For random vertical slices through a circular plume, the measured horizontal dimension will be greater than 50% of the actual diameter 87% of the time just from geometric considerations. However, since the lidar can usually make several vertical scans through the same plume and the largest diameter is taken, the actual measurements probably have less than a 10% error. Plumes are most visible to the lidar during mid and late morning when the inversion is rising most rapidly. The layer below the inversion becomes well mixed once a strong capping inversion is reached. Therefore, the great majority of plume sizes were measured at heights below 1 km and during a time when the boundary layer was rapidly evolving.

The lidar observations reveal a wide range of sizes with the following features. The observed dome-like structures exhibit diameters of 600–1500 m. This is in agreement with radar studies (e.g., Konrad, 1970). The plume structures are considerably smaller in diameter with a range of 100–800 m with the majority in the 200–500 m interval. Fig. 3 shows a probability distribution of plume top height z_p plotted as a function of plume diameter D. This plot was generated from measurements on 16 days distributed throughout the year. A total of 464 plumes were measured. We find that the diameter does not change significantly with height for any given plume. However, Fig. 3 shows that the average diameter increases as the tops of the plumes, determined largely by the inversion height, get higher. These two facts are in qualitative agreement with the plume model of Telford (1966, 1970, 1972, 1975). Plume merging may be responsible for the increase in average plume size with inversion rise. We have observed several instances when this occurred. The lidar observations of cell size shown on the graph encompass the entire range which has been reported by other investigators. This suggests that the differences in reported plume sizes may be due to spatial and/or temporal sampling limitations.

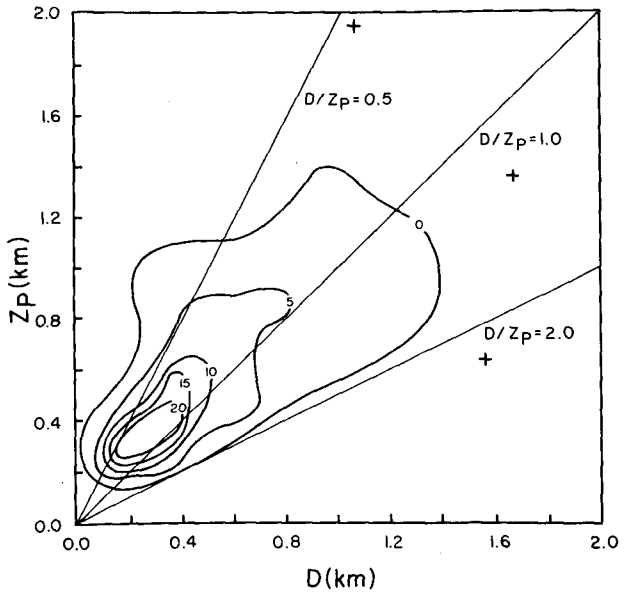

FIG. 3. Plume size versus plume height for lidar observations of convection over land. Contours show the number of plumes observed with height z_p and diameter D in 100 m×100 m size intervals. Crosses give location of individual plumes observed outside the zero probability contour.

The observed aspect ratio $A = D/Z_p$ of the majority of plumes is between 0.5 and 1.5 with an average value slightly less than 1.0. Willis and Deardorff (1976) found an average aspect ratio of 1.3 in a tank study. This falls within the range of the lidar measurements although it is slightly larger. In this tank study, the convective layer was allowed to reach a quasi-steady state. In contrast, the bulk of the lidar measurements were taken during periods of rapid growth in the boundary layer. This may account for the small difference in average aspect ratio.

Fig. 3 also shows that along a line of constant aspect ratio the probability of occurrence of plumes decreases above a height of about 250 m. This is a reflection of the average height of the capping inversion when the data were collected.

In order to see whether the urban nature of the surface affected the measured aspect ratios, lidar measurements were taken over Lake Mendota during Canadian cold air outbreaks in the late fall of 1976. Lake Mendota is located on the northwest side of Madison and is 5–7 km in diameter. The lake provided a flat and approximately isothermal heat source for convection. Measurements of aspect ratio taken on three separate days show essentially the same behavior as indicated in Fig. 2.

5. Measurement of convective circulation patterns: Case studies

Fig. 4 shows a time sequence of five RHI pictures taken on 29 April 1976 near 1045 CDT over urban terrain. The interval between frames was 80 s and the mean wind was less than 2 m s^{-1}. At the start of the sequence, skies were mostly clear and a few small cumulus clouds were beginning to form. These pictures clearly show two convective cells located approximately 3.5 and 6 km from the lidar. A small cumulus begins to form on the top of the cell at 6 km in frame 4b. This cumulus is responsible for the dark area in the upper left-hand corner of this and subsequent frames since the lidar cannot penetrate clouds.

The McIDAS system was used to map the circulation pattern in the layer by measuring the displacements of individual features in these frames. Fig. 5 shows frame 4a with these wind vectors superimposed. The base of

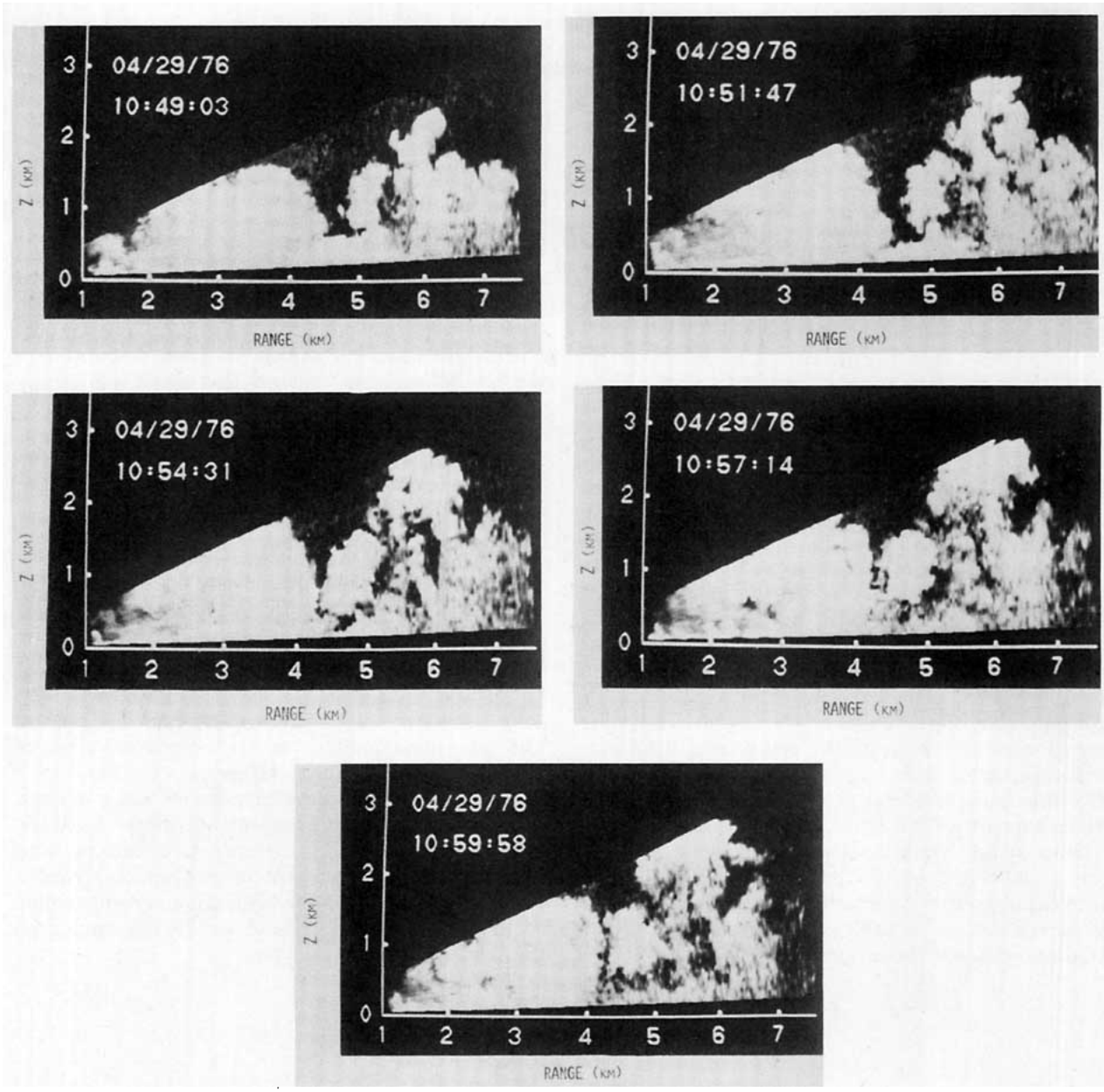

FIG. 4. Photographs of lidar range versus height displays showing the development of convective structure in a visually clear atmosphere on 29 April 1976. The white areas are those where aerosol density is somewhat greater than the ambient background. Observation times are shown in the figures. Notice the rapid development of the plume at a range of 6 km. Frames 4b–4e show a small cumulus cloud which has developed at the top of this plume in the time interval between frames 4a and 4b. The cloud quickly extinguishes the laser pulse causing a dark shadow at the upper right.

each vector is located at the position where the velocity was measured. These vectors indicate that most features are being advected slowly to the right in Fig. 5.

An interesting feature of the velocity field in Fig. 5 is that the strongest rising motion occurs on the upwind side of the cells. Aircraft and tower observations by Warner and Telford (1964, 1967), Lenschow (1970) and Kaimal and Businger (1970) indicate that the hottest part of a convective plume is on the upwind side. This is compatible with the present lidar observations since the hottest part of the plume should coincide with the region of greatest vertical velocity. The compensating downdraft for both cells is considerably weaker and seems to occur preferentially on the downwind side of the cell. A model of a convective cell with rising motion upwind and sinking motion downwind is shown schematically in Fig. 6. This circulation has a sense of rotation about a horizontal axis perpendicular to the mean flow, suggesting that the rotational part of the circulation is dynamically driven by the shear flow.

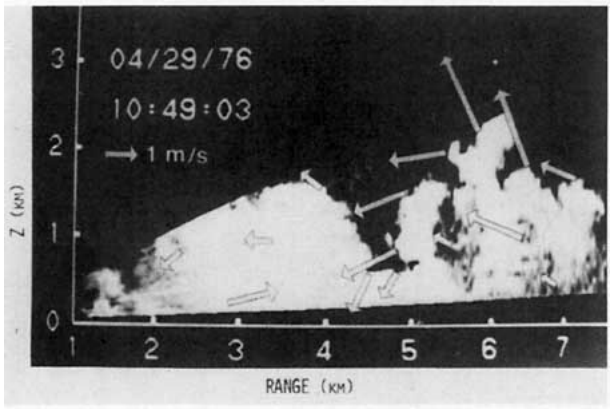

FIG. 5. Wind vectors obtained from the displacement of plume structure in the 160 s time interval between frames 4a and 4b.

This type of circulation pattern has been observed by others in cumulus clouds (e.g., Byers, 1965, p. 178). The lidar data shows that this pattern exists before cloud formation has begun.

The observations of Fig. 4 also have implications for the parameterizations of vertical fluxes in convective boundary layers. Both cells shown in Fig. 4a have circulations which encompass nearly the entire depth of the boundary layer. The appropriate length scale of these vertical mixing processes must therefore be comparable to the inversion height z_i. Previous studies, e.g., Deardorff (1972) and Kaimal *et al.* (1976), have indicated that z_i is an important parameter in convective situations. The lidar depiction of convection gives visual support for this hypothesis.

Since typical vertical velocities in a convective field are around 0.1–1 m s^{-1}, the vertical mixing of heat, momentum, water vapor, etc., is very rapid. In fact, vertical fluxes are probably entirely determined by the transport processes occurring in the viscous and surface layers and by the rate of entrainment at the inversion. This is compatible with measurements of vertical profiles of wind and temperature which show that vertical gradients are weak or nonexistent in convective layers except near the top or bottom of the layer (see Clarke, 1970; Kaimal *et al.*, 1976).

Fig. 4 also visually illustrates the problems of using stationary *in situ* instruments to measure fluxes and other turbulence quantities in light wind convective situations. Over the entire period which these frames cover (~10 min), the convective cells have moved horizontally less than 0.5 km. Since the spacing between the two cells is about 3 km, an *in situ* sensor would sample about 1 cell h^{-1}. Any statistical description of the convective layer requires the sampling of many cells. But, during the morning when the boundary layer is evolving rapidly, the statistical description of the layer may change over the time period of 1 h. Obviously, an *in situ* sensor will fail to adequately describe the layer in such a situation.

6. Conclusions

These preliminary results indicate that a high spatial resolution lidar system with scanning capabilities is a powerful tool for the observation of the convective boundary layer. These lidar observations of convective motions show the following:

1) Convective plumes have roots near the surface. The lidar data indicate that the preferred form of convective cells are plumes rather than bubbles.

2) The observed plumes have a wide range of sizes, the majority having an aspect ratio between 0.5 and 1.5.

3) The lidar is able to observe circulation patterns in and around convective structures. These observations indicate that these cells have a maximum rising motion on the upwind side of the cell and sinking motion on the downwind side.

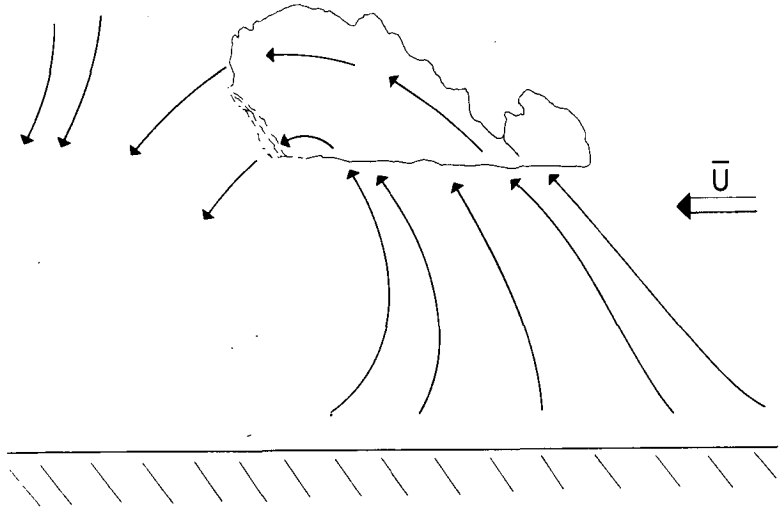

FIG. 6. Schematic view of the flow pattern observed around a developing fair weather cumulus cloud.

Acknowledgments. We would like to thank Professor James Weinman for his suggestions during the course of this work. This work was partially funded by USAROD grant DAAG29-76-C-0156. The senior author (Kunkel) was supported by a National Science Foundation fellowship during part of the work.

REFERENCES

Byers, H. R., 1965: *Elements of Cloud Physics*. University of Chicago Press, 191 pp.

Clarke, R. H., 1970: Observational studies in the atmospheric boundary layer. *Quart. J. Roy. Meteor. Soc.*, **96**, 91–114.

Deardorff, J. W., 1972: Numerical investigations of neutral and unstable planetary boundary layers. *J. Atmos. Sci.*, **29**, 91–115.

Hall, F. F., 1972: Temperature and wind structure studies by acoustic echo-sounding. *Remote Sensing of the Troposphere*, Govt. Printing Office, Chap. 18.

Hardy, K. R., and H. Ottersten, 1969: Radar investigations of convective patterns in the clear atmosphere. *J. Atmos. Sci.*, **26**, 666–672.

Kaimal, J. C., and J. A. Businger, 1970: Case studies of a convective plume and a dust devil. *J. Appl. Meteor.*, **9**, 612–620.

——, J. C. Wyngaard, D. A. Haugen, O. R. Coté, Y. Izumi, S. J. Caughey and C. J. Readings, 1976: Turbulence structure in the convective boundary layer. *J. Atmos. Sci.*, **33**, 2152–2169.

Konrad, T. G., 1970: The dynamics of the convective process in clear air as seen by radar. *J. Atmos. Sci.*, **27**, 1138–1147.

——, and F. L. Robison, 1972: Simultaneous measurements of radar reflectivity and refractive index spectra in clear air convection. *J. Appl. Meteor.*, **11**, 1114–1119.

——, and ——, 1973: Development and characteristics of free convection in the clear air as seen by radar and aircraft. *J. Appl. Meteor.*, **12**, 1284–1294.

Kunkel, K. E., E. W. Eloranta and J. A. Weinman, 1975: Visualization of eddies in the planetary boundary layer by means of lidar. *Preprints Int. Conf. Environ. Sensing and Assessment*, Las Vegas, Amer. Meteor. Soc.

Lenschow, D. H., 1970: Airplane measurements of planetary boundary layer structure. *J. Appl. Meteor.*, **9**, 874–884.

Rowland, J. R., 1973: Intensive probing of a clear air convective field by radar and instrumented drone aircraft. *J. Appl. Meteor.*, **12**, 149–155.

——, 1976: Clear air convective behavior revealed by radar chaff. *J. Appl. Meteor.*, **15**, 521–526.

Scorer, R. S., and F. H. Ludlam, 1953: Bubble theory of penetrative convection. *Quart. J. Roy. Meteor. Soc.*, **79**, 94–103.

Smith, E., 1975: The McIDAS system. *IEEE Trans. Geosci. Electron.*, **GE-13**, No. 3.

Telford, J. W., 1966: The convective mechanism in clear air. *J. Atmos. Sci.*, **23**, 652–666.

——, 1970: Convective plumes in a convective field. *J. Atmos. Sci.*, **27**, 347–358.

——, 1972: A plume theory for the convective field in clear air. *J. Atmos. Sci.*, **29**, 128–134.

——, 1975: The effect of compressibility and dissipation heating on boundary layer plumes. *J. Atmos. Sci.*, **32**, 108–115.

——, and J. Warner, 1964: Fluxes of heat and vapor in the lower atmosphere derived from aircraft observations. *J. Atmos. Sci.*, **21**, 539–548.

Vulf'son, N. L., 1961: Convective Motions in a Free Atmosphere. Moscow, Gidrometerizdat. [English translation from NTIS, Ref. No. OTS64-11017.]

Warner, J., and J. W. Telford, 1963: Some patterns of convection in the lower atmosphere. *J. Atmos. Sci.*, **20**, 313–318.

——, and —— 1967: Convection below cloud base. *J. Atmos. Sci.*, **24**, 374–382.

Willis, G. E., and J. W. Deardorff, 1976: Visual observations of horizontal planforms of penetrative convection. *Preprints Third Symp. Atmospheric Turbulence, Diffusion and Air Quality*, Raleigh, Amer. Meteor. Soc., 9–12.